Korean J Physiol Pharmacol 2025;29(1):9-19
https://doi.org/10.4196/kjpp.24.115

KJPP

Original Article

Fine particulate matter induces osteoclast-mediated bone loss in mice

Hye Young Mun[1], Septika Prismasari[1], Jeong Hee Hong[2], Hana Lee[3], Doyong Kim[3], Han Sung Kim[3], Dong Min Shin[4], and Jung Yun Kang[1,*]

[1]Department of Dental Hygiene, College of Software and Digital Healthcare Convergence, Yonsei University, Wonju 26493, [2]Department of Physiology, College of Medicine, Gachon University, Lee Gil Ya Cancer and Diabetes Institute, Incheon 21999, [3]Department of Biomedical Engineering, College of Software and Digital Healthcare Convergence, Yonsei University, Wonju 26493, [4]Department of Oral Biology, Yonsei University College of Dentistry, Seoul 03722, Korea

ARTICLE INFO

Received April 11, 2024
Revised July 19, 2024
Accepted August 19, 2024
Published online October 31, 2024

***Correspondence**
Jung Yun Kang
E-mail: hannahkang@yonsei.ac.kr

Key Words
Air pollution
Bone and bones
Osteoclasts
Particulate matter
X-ray microtomography

ABSTRACT Fine particulate matter (FPM) is a major component of air pollution and has emerged as a significant global health concern owing to its adverse health effects. Previous studies have investigated the correlation between bone health and FPM through cohort or review studies. However, the effects of FPM exposure on bone health are poorly understood. This study aimed to investigate the effects of FPM on bone health and elucidate these effects *in vitro* and *in vivo* using mice. Micro-CT analysis *in vivo* revealed FPM exposure decreased bone mineral density, trabecular bone volume/total volume ratio, and trabecular number in the femurs of mice, while increasing trabecular separation. Histological analysis showed that the FPM-treated group had a reduced trabecular area and an increased number of osteoclasts in the bone tissue. Moreover, *in vitro* studies revealed that low concentrations of FPM significantly enhanced osteoclast differentiation. These findings further support the notion that short-term FPM exposure negatively impacts bone health, providing a foundation for further research on this topic.

INTRODUCTION

In 2019, 99% of the global population resided in areas that failed to meet the World Health Organization air quality guidelines. Worldwide, an estimated 4.2-million premature deaths per year are attributed to the exposure to fine particulate matter (FPM) [1], which is a major component of air pollution that is associated with significant health risks [2]. Based on the aerodynamic diameter, particulate matter is categorised as coarse (< 10 μm; PM_{10}), fine (< 2.5 μm; $PM_{2.5}$), and ultrafine (< 0.1 μm; $PM_{0.1}$) particles [3]. Compared to PM_{10}, other FPM, especially $PM_{2.5}$, contain higher concentrations of harmful metals such as arsenic (As), cadmium (Cd), chromium (Cr), and lead (Pb) [4]. Smaller particles have a higher capability of penetrating the lungs and travelling deeper into cellular tissues and/or the circulatory system, eventually entering the bloodstream and circulating throughout the body to induce other organ-related issues [5]. Therefore, particulate matter can reach the bones *via* the bloodstream.

Numerous studies have demonstrated FPM-induced adverse health effects that are mediated through the induction of oxidative stress and inflammatory responses, which can contribute to lung diseases, cardiovascular diseases, diabetes, and allergies [6]. However, most studies have primarily focused on the respiratory tract (bronchi and lungs), whereas limited research has been conducted on other parts of the body. FPM exposure stimulates the production of inflammatory cytokines and activates oxidative stress signalling, which potentially contributes to the pathogenesis of bone diseases [7,8]. In 2021, a meta-analysis that included

Author contributions: H.Y.M. and J.Y.K. conceptualized and designed the study and acquired, analyzed, and interpreted data. Experiments were performed by H.Y.M., S.P., H.L., D.K., and H.S.K. H.Y.M., S.P., and J.Y.K. drafted the manuscript and acquired data. J.H.H. and D.M.S revised the manuscript critically for important intellectual content. J.Y.K. contributed to the funding acquisition and final approval of the published version and are responsible for all aspects of the work as regards the accuracy and integrity of the study.

86 studies revealed that the global prevalence of osteoporosis was 18.3 (95% confidence interval 16.2–20.7) [9]. Osteoporosis is a prevalent bone disease that is characterised by an imbalance between osteoblasts, which undertake osteogenesis, and osteoclasts, which effect bone resorption during remodelling. An imbalance can occur secondary to osteoclast overactivation, which increases bone resorption relative to bone formation, or, conversely, from reduced osteoblastic activity [10]. A cohort study of the associations among FPM exposure, bone mineral density (BMD), and osteoporosis showed that exposure to higher-level FPM pollution was associated with lower BMD and higher prevalence of osteoporosis [11]. In young adults, ambient air pollution was linked to lower bone mineral content [12]. Furthermore, a data-driven analysis of studies that examined the effects and mechanisms of FPM on the bone indicated potentially negative effects [13]. However, as the previous studies that investigated and suggested a relationship of FPM with bone health were predominantly cohort or review studies, direct experimental evidence of this association is lacking. Therefore, this study aimed to investigate the effects of FPM on mouse bones.

METHODS

Mice, chemicals, and materials

Six-week-old male ICR mice from Koatech were housed under controlled conditions (12-h light/dark cycle, appropriate temperature, and humidity) prior to the commencement of the experiment. This study was conducted using ICR mice because they share several genetic and physiological similarities, including bone structure and metabolism, with humans. Furthermore, as ICR mice are outbred, they have diverse genetic backgrounds, which provide a more representative model of the general population and, thereby, reduce the influence of genetic anomalies on experimental outcomes [14]. FPM mixtures were obtained from the National Institute of Standards and Technology (SRM 2786). Lipopolysaccharide (LPS), isolated from *Escherichia coli* (0111:B4; EMD), was dissolved in phosphate-buffered saline (PBS; Welgene) before use. The tartrate-resistant acid phosphatase (TRAP) assay kit (Sigma-Aldrich Inc.) was used to quantify osteoclast differentiation. Macrophage colony-stimulating factor (M-CSF) was obtained from Peprotech, and recombinant mouse TRANCE/TNFSF11/receptor activator of nuclear factor kappa B ligand (RANKL) was acquired from R&D Systems. Foetal bovine serum (FBS), penicillin–streptomycin, and trypan blue (0.4%) were purchased from Gibco-BRL. Minimum essential medium alpha modification (α-MEM) was obtained from Cytiva-Hyclone, and 4% paraformaldehyde was obtained from Bylabs. Cell viability was assessed using the CellTiter 96 Aqueous One Solution Cell Proliferation Assay (Promega).

Experimental design and animal models

To investigate whether FPM directly affects the bone through the bloodstream, we established an animal model wherein FPM was administered intraperitoneally. Fig. 1A shows the timeline and sequence of *in vivo* experiments. All animal experiments were approved by the Institutional Animal Care and Use Committee of the Yonsei University (licence number: YWCI-202308-015-02). Animal care and experimentation were conducted in accordance with the guidelines of the Institutional Animal Care and Use Committee of Yonsei University. The ICR mice were randomly assigned to three treatment groups (control, n = 5; FPM, n = 7; and LPS, n = 3) based on their body weight. *Via* intraperitoneal (IP) injection, the control group received 10 ml/kg PBS, whereas the FPM and LPS groups received 7.5 and 5 mg/kg, respectively. The FPM concentrations employed in this study were established based on findings from previous research conducted in Japan. To ensure realistic inhalation and accumulation rates mimicking real-world human breathing patterns, the concentrations were meticulously adjusted in the mouse model. The 7.5 mg/kg dose selected for this study, which exceeds ambient $PM_{2.5}$ concentrations, constitutes an approximately tenfold dose [15,16] that was calculated to simulate human exposure levels and their corresponding health effects. In another study, 7.5 mg/kg FPM was injected into maternal rats intraperitoneally as an experimental exposure route. Lung damage occurred in foetal rats, which suggested that FPM may affect the bone *via* the bloodstream [17,18]. IP injections are widely used in toxicological studies of FPM. This method is particularly effective because it permits FPM distribution throughout the body, mimicking systemic exposure. Eventually, FPM enters the bloodstream and circulates throughout the body, leading to issues in other organs, including the bone. Compared to other routes, IP injection facilitates more efficient uptake and distribution of particles, which makes it possible to observe the bone-related impact of short-term FPM exposure [19]. Therefore, this study used IP injections in the animal experiments. Throughout the experiment, the body weight of the mice was measured every 3 days for all treatment groups, and the body weight measurements of the different groups on Day 12, and 19 are shown in Fig. 1B. Throughout the experiment, no significant differences in body weight were observed. The body weights of the mice were within the normal range. Subsequently, differences among all the mice were evaluated from before to after the experiment. All the mice used in this study received appropriate humane care, including pain relief.

Micro-computed tomography (micro-CT)

To evaluate microstructural changes in the femoral bone, the right hindlimb of each mouse was scanned using micro-CT (Skyscan1176; Bruker microCT) on days 0, 12, and 19. All animals were anaesthetised with isoflurane (Hanaph) to minimise

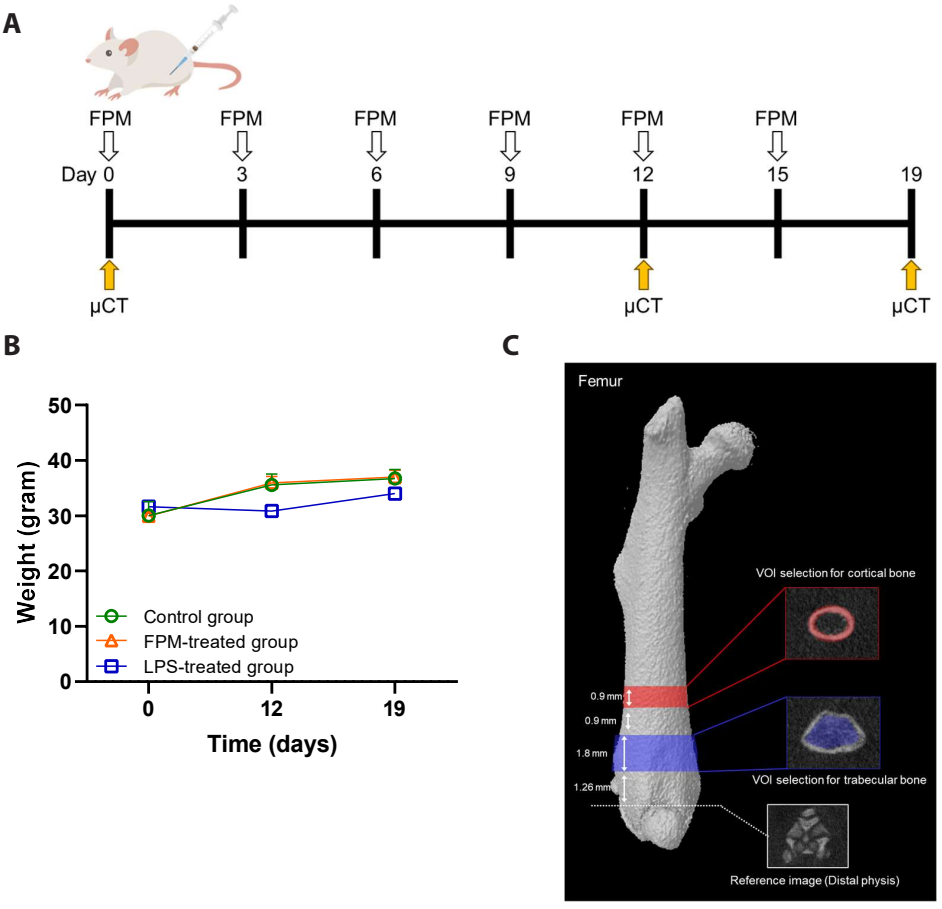

Fig. 1. Experimental design of fine particulate matter (FPM)-induced effects in a mouse model. (A) Strategic abstract of the experimental processes. Mice were divided into three independent groups (control group, n = 5, FPM-treated group, n = 7, and lipopolysaccharide [LPS]-treated group, n = 3). FPM (7.5 mg/kg) was administered every 3 days to ICR mice intraperitoneally for 12 or 19 days. The control group received phosphate-buffered saline (PBS, 10 ml/kg) instead, and LPS (5 mg/kg) was used as a positive control. (B) Body weight during the experiment. No significant change in body weight was observed between the intra- group during the FPM administration period. (C) Schematic representation of the micro-computed tomography (CT) scanning procedures for the assessment of microstructure of the femur. Overview of volume-of-interest (VOI) selection for the femur. VOI for the trabecular bone at distal metaphysis is shown in the red panels. VOI for the cortical bone at mid-diaphysis is shown in the blue panel. Scale bar, 1 mm.

movement during scanning. A 1-mm aluminium filter was used to evaluate the change in the shape of the bone tissue under the following parameters: voltage 75 kV, current 333 μA, resolution 18 μm, exposure time 260 ms, and rotation step 0.7 degree. The acquired raw data were translated into two-dimensional cross-sectional grayscale image slices using NRecon software (Brucker micro-CT, ver.1.6.9.3). The reconstructed images were geometrically aligned using DataViewer software (Brucker micro-CT, ver.1.5.1.2). For morphometric analysis, the bone-structural parameters were measured using a CT analyser (CT-AN ver.1.10.9.0, Brucker). Both before and after treatment, the right femur of each mouse was imaged using a microtomography system. Fig. 1C depicts an overview of the femoral volume-of-interest (VOI) selection. The VOI and region of interest settings used in the analysis were based on the manufacturer's instructions as well as previously reported methods [20,21]. The VOI for the trabecular bone was set by designating a section 1.26 mm away from the distal physis to a height of 1.8 mm (100 image slices; Fig. 1C). The trabecular bone-related detection parameters included: BMD (g/cm^3), reflecting the mineral range of bone tissue; bone volume/total volume ratio (BV/TV, %), reflecting the ratio of bone volume to total volume; trabecular thickness (Tb.Th, μm), indicating the average thickness of the trabeculae; bone surface-to-bone volume ratio (BS/BV, mm^{-1}), representing the ratio between bone surface area and volume; trabecular separation (Tb.Sp, μm), indicating the distance between trabeculae; and the trabecular number (Tb.N, mm^{-1}), representing the number of trabeculae per unit length. The VOI for cortical bone was set by designating a section situated 3.96 mm away from the distal physis to a height of 0.9 mm (50 image slices; Fig. 1C). The detection parameters related to the cortical bone were: BMD (g/cm^3); cross-sectional thickness (Cs.Th, mm), representing the thickness of the cortical bone; BV (cm^3), indicating the volume of the cortical bone; and mean polar moment of inertia (MMI, mm^4), indicating the ability to resist torsion.

Histological examination

The left femur was fixed in 4% paraformaldehyde for 2 days at 4°C; decalcified in 10% ethylenediaminetetraacetic acid for 2 weeks; and then dehydrated with ethanol, clarified with xylene, and embedded in paraffin. The paraffin-embedded sections were cut and stained with haematoxylin and eosin (H&E) and TRAP staining kit (Wako) according to the manufacturer's instructions. Histological changes in the femur were observed under a light microscope (Olympus CKX53). The resulting images were analysed using ImageJ software.

Cell cultures

Bone marrow-derived macrophages (BMMs) were isolated from the femurs and tibiae of 6-week-old male ICR mice by flushing with histopaque density gradient centrifugation according to a previously described protocol [22]. The BMMs were cultured in α-MEM supplemented with 10% FBS, 1% penicillin–streptomycin with M-CSF (30 ng/ml), and RANKL (50 ng/ml) for 5 days, with medium replacement every second day. In a 96-well plate, the BMMs were seeded at a density of 5×10^4 cells/well, exposed to FPM at concentrations of 0, 3.125, 6.25, and 12.5 μg/ml, and incubated at 37°C in 5% CO_2. The concentration of FPM was determined by referring to the concentration used in previous studies [23].

Cell viability assay

Using an 3-(4,5-dimethylthiazol-2-yl)-5-(3-carboxymethoxyphenyl)-2-(4-sulfophenyl)-2H-tetrazolium (MTS) assay, cell viability was assessed for BMMs seeded in 96-well plates containing α-MEM supplemented with 10% FBS, 1% penicillin–streptomycin, and M-CSF (30 ng/ml). To these plates, various concentrations of FPM (0, 3.125, 6.25, and 12.5 μg/ml) were added, and the cells were incubated for 2 days at 37°C in 5% CO_2. Next, the cells were incubated for 1 h with the MTS assay solution, and absorbance at 490 nm was measured for each well using an absorbance microplate reader (SpectraMax ABS reader) to determine cell viability.

TRAP assay

The BMMs were stimulated with various concentrations of FPM (0, 3.125, 6.25, and 12.5 μg/ml) or PBS, M-CSF (30 ng/ml), and RANKL (50 ng/ml). After 5 days of culture, the cells were stained using a TRAP assay kit according to the manufacturer's instructions. The plates were photographed using a light microscope (Olympus CKX53), and the staining intensity was quantified using ImageJ software (National Institutes of Health).

Statistical analysis

All data were presented as the mean ± standard deviation of three or more independent experiments. The Shapiro–Wilk test was used to test the normality of data distribution, and the Levene's test was applied to assess the homogeneity of variances. If the assumptions of normal distribution and homogeneity of variances were met, a one-way analysis of variance (ANOVA) was conducted to determine the differences between the experimental groups. *Post-hoc* analysis was performed using Tukey's test. If the assumptions of normal distribution or homogeneity of variances were not met, the Kruskal–Wallis test was used. This was followed by multiple comparisons with Bonferroni correction. To confirm the percentage change (%) in the parameters measured *via* micro-CT after the application of FPM in mice, the values from each group at 12 or 19 days after application were normalised to the mean values before application. The percentage change (%) was calculated using previously described methods [24]. The results are presented as the mean relative percentage difference between each group, normalised to the baseline values before application. All data were analysed using SPSS (SPSS Statistics 26.0; IBM Co.). Figures were created using GraphPad Prism 8 software (*$p < 0.05$; **$p < 0.01$; ***$p < 0.001$; NS, not significant).

Table 1. Structural parameters of trabecular and cortical bone calculated from micro-CT images in mice

Days	Day 0	Day 12			Day 19		
Group	Pre-treatment	Control	FPM	LPS	Control	FPM	LPS
Trabecular bone							
BMD (g/cm^3)	0.19 ± 0.03	0.19 ± 0.04	0.16 ± 0.04	0.10 ± 0.02**	0.16 ± 0.04	0.14 ± 0.03**	0.09 ± 0.02**
BV/TV (%)	42.28 ± 10.35	39.02 ± 12.93	32.11 ± 12.10	12.34 ± 4.06**	31.27 ± 11.10	25.59 ± 10.19**	13.79 ± 3.92**
Tb.Th (mm)	0.13 ± 0.02	0.13 ± 0.02	0.11 ± 0.02	0.10 ± 0.01	0.12 ± 0.02	0.11 ± 0.02	0.10 ± 0.01
BS/BV (1/mm)	29.94 ± 5.11	30.93 ± 6.08	35.62 ± 8.39	44.18 ± 4.25**	34.33 ± 6.97	38.62 ± 8.99*	40.98 ± 3.59*
Tb.Sp (mm)	0.20 ± 0.05	0.21 ± 0.06	0.23 ± 0.05	0.42 ± 0.11**	0.26 ± 0.06	0.34 ± 0.08**	0.51 ± 0.13**
Tb.N (1/mm)	3.30 ± 0.39	3.00 ± 0.69	2.71 ± 0.71	1.26 ± 0.41**	2.52 ± 0.63	2.25 ± 0.68**	1.33 ± 0.30**
Cortical bone							
BMD (g/cm^3)	0.67 ± 0.02	0.68 ± 0.04	0.67 ± 0.03	0.66 ± 0.03	0.65 ± 0.02	0.64 ± 0.03	0.65 ± 0.05
Cs.Th (mm)	0.18 ± 0.02	0.19 ± 0.02	0.18 ± 0.03	0.16 ± 0.02	0.18 ± 0.02	0.17 ± 0.03	0.15 ± 0.03
Ct.BV (mm^3)	0.99 ± 0.09	1.10 ± 0.11	1.00 ± 0.14	0.88 ± 0.05	1.03 ± 0.13	0.91 ± 0.14	0.80 ± 0.12
MMI (mm^4)	0.78 ± 0.11	0.92 ± 0.12	0.82 ± 0.13	0.71 ± 0.07	0.84 ± 0.15	0.73 ± 0.13	0.64 ± 0.06

Values are presented as mean ± standard deviation. Pre-treatment group (Day 0) *vs*. control group, FPM-treated group, LPS-treated group. *$p < 0.05$, **$p < 0.01$, Kruskal–Wallis test. CT, computed tomography; FPM, fine particulate matter; LPS, lipopolysaccharide; BMD, bone mineral density; BV/TV, bone volume/total volume; Tb.Th, trabecular thickness; BS/BV, bone surface to bone volume ratio; Th.Sp, trabecular separation; Tb.N, trabecular number; Cs.Th, cross-sectional thickness; Ct.BV, cortical bone volume; MMI, mean polar moment of inertia.

https://doi.org/10.4196/kjpp.24.115

RESULTS

FPM-induced femoral trabecular bone loss in mice

To ascertain the effects of FPM on the femoral trabecular bone of mice, the mice were treated with FPM and examined using micro-CT after 12 and 19 days; the LPS group served as a positive control for comparison. To compare the bone changes from the pre-treatment to post-treatment evaluations, the results were normalised to the baseline values before application, and inter-group comparisons were performed. The absolute values of the experimental results are shown in Table 1. In the FPM-treated group, we observed significant bone loss over time (representative image in Fig. 2A). Relative changes in bone density and structure over time in the trabecular bone were observed in the transverse and coronal sections. In the transverse section of the femur, only the trabecular bone (blue-shaded) area was analysed. On Day 19, compared to the baseline pre-treatment values, FPM-treated and LPS-treated groups showed a significant decrease in BMD (Fig. 2B), BV/TV (Fig. 2C), and Tb.N (Fig. 2G) values, as well as a sig-

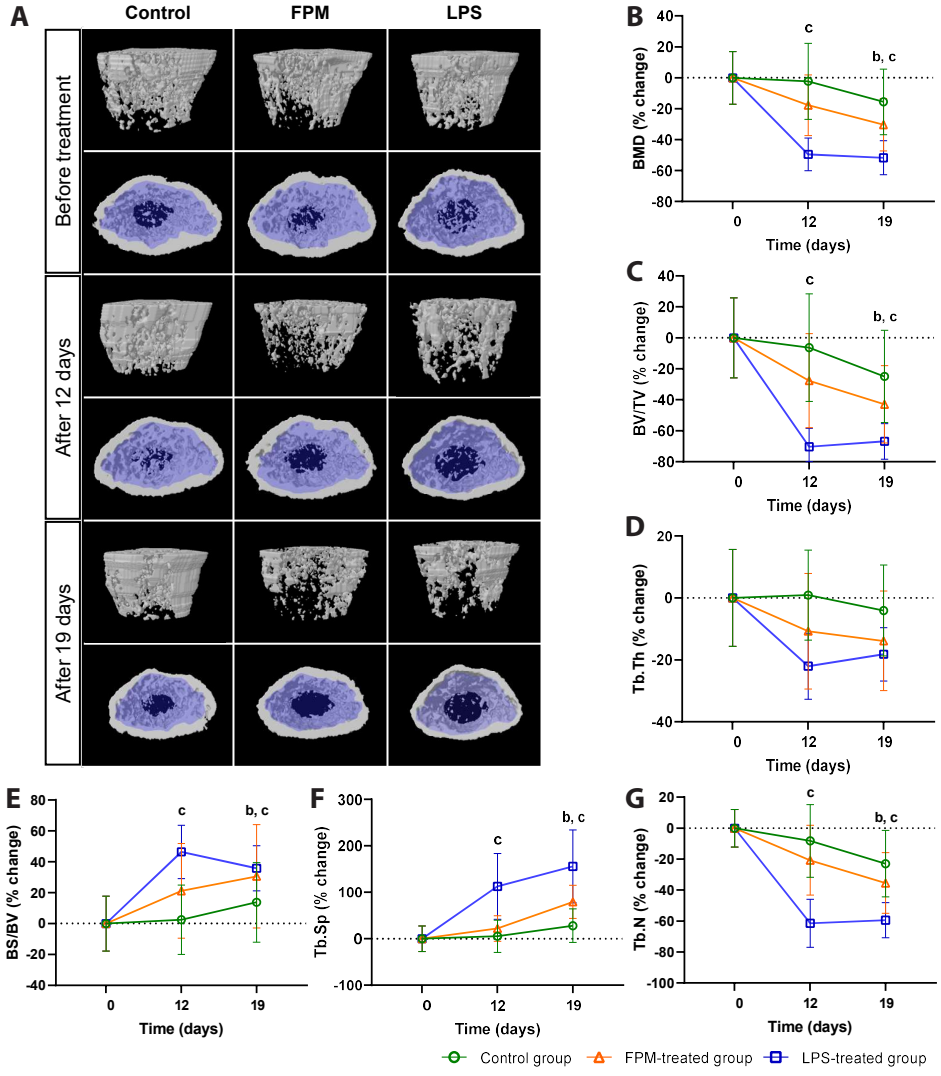

Fig. 2. Micro-CT analysis to investigate the effects of fine particulate matter (FPM) on the femoral trabecular bone of mice. (A) Representative micro-CT coronal (top) and transverse (bottom) scans of the trabecular bone from each group. Mean changes in trabecular bone density and structure over time were measured (control group, n = 5, FPM-treated group, n = 7, and LPS-treated group, n = 3). In the transverse section of the femur, the trabecular bone is shaded in blue, and only the trabecular bone area was analysed. (B–G) Mean percentage change of trabecular bone parameters in the treatment groups based on the pre-treatment value at Day 0. Treatment commenced in 6-week-old mice and was terminated after 19 days. Significant differences between each group normalized to the baseline values before application are noted ($p < 0.05$, Kruskal–Wallis test): [a]pre-treatment group (PTG) *vs*. control group, [b]PTG *vs*. FPM-treated group, [c]PTG *vs*. LPS-treated group. (B) Bone mineral density (BMD), (C) bone volume/total volume (BV/TV), (D) trabecular thickness (Tb.Th), (E) bone surface to bone volume ratio (BS/BV), (F) trabecular separation (Tb.Sp), and (G) trabecular number (Tb.N). The control group received PBS (10 ml/kg), FPM-treated group received PBS-diluted FPM (7.5 mg/kg), and LPS-treated group received lipopolysaccharide (5 mg/kg). Bars represent mean ± standard deviation. LPS, lipopolysaccharide; CT, computed tomography; PBS, phosphate-buffered saline.

nificant increase in the BS/BV and Tb.Sp value (Fig. 2E, F) (all $p < 0.05$). Both the positive control and LPS-treated groups showed significant changes from Day 12. For parameters that showed significant changes, the FPM-treated group exhibited values between those of the control and LPS-treated groups. Furthermore, no significant change was observed between the pre-treatment and control groups. Although not statistically significant, Tb.Th (Fig. 2D) showed a decreasing and increasing trend over time, respectively, due to FPM. Analysis of the structural parameters of the trabecular bone using a micro-CT system revealed significant

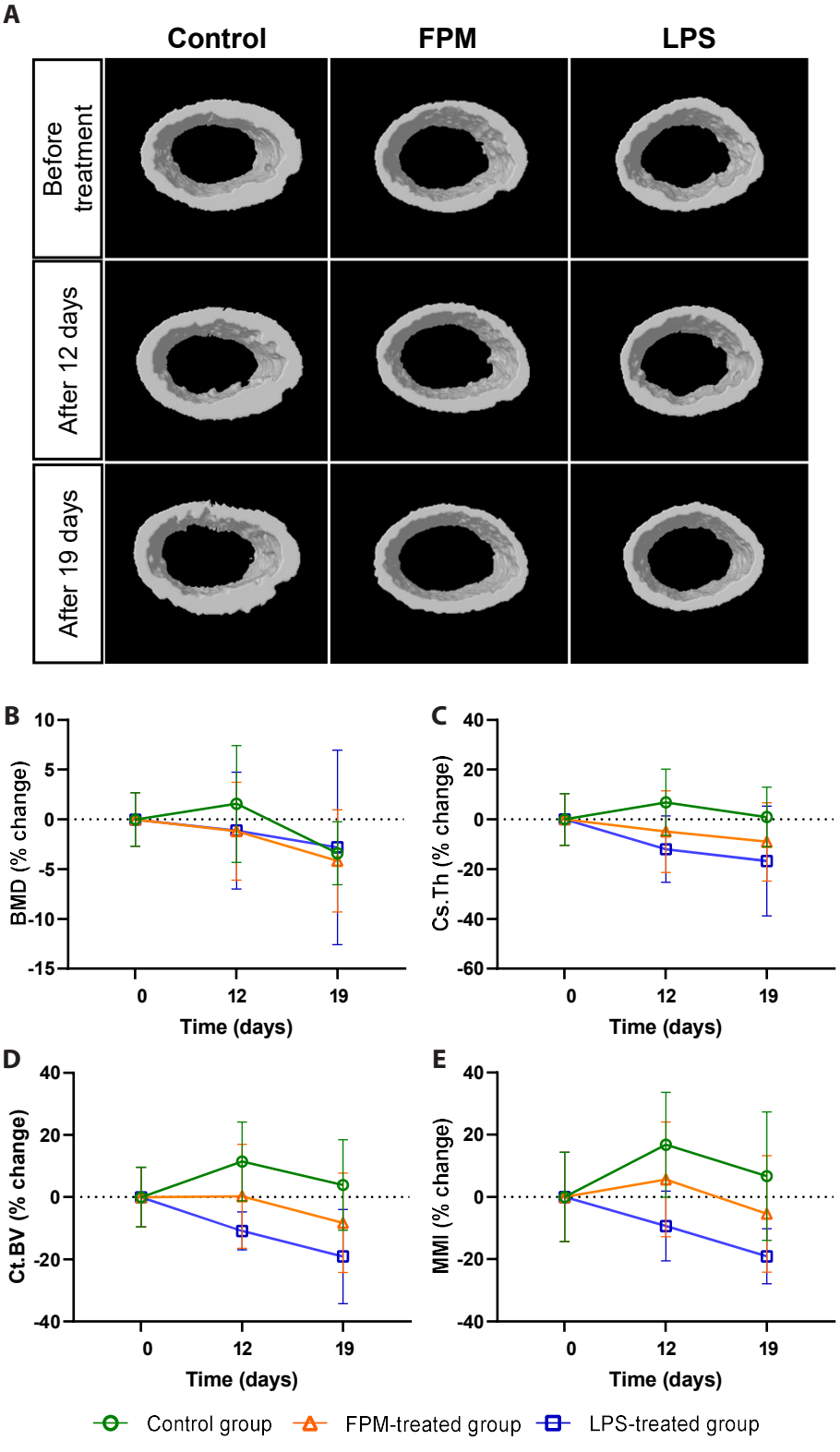

Fig. 3. Micro-CT analysis to investigate the effects of fine particulate matter (FPM) on the femoral cortical bone in mice. (A) Representative micro-CT transverse cross-sectional images of the cortical bone from each group. Mean changes in cortical parameters over time were measured (control group, n = 5, FPM-treated group, n = 7, and LPS-treated group, n = 3). (B, C) Mean percentage changes in cortical bone parameters in the treatment groups based on the pre-treatment value at Day 0. Treatment commenced in 6-week-old mice and was stopped after 19 days. Significant differences between each group normalized to the baseline values before application are noted ($p < 0.05$, Kruskal–Wallis test): (B) Bone mineral density (BMD), (C) cross-sectional thickness (Cs.Th), (D) cortical bone volume (Ct.BV), and (E) mean polar moment of inertia (MMI). The control group received PBS (10 ml/kg), FPM-treated group received PBS-diluted FPM (7.5 mg/kg), and LPS-treated group received lipopolysaccharide (5 mg/kg). Bars represent mean ± standard deviation. LPS, lipopolysaccharide; CT, computed tomography; PBS, phosphate-buffered saline.

bone loss in the FPM-exposed group.

FPM does not induce significant changes in the femoral cortical bone in mice

To investigate the effects of FPM on the femoral cortical bone of mice, mice were treated with FPM and examined *via* micro-CT after 12 and 19 days. The femoral diaphysis did not show significant intergroup differences in cortical microarchitecture (Fig. 3A). While significant changes were observed in the trabecular bone, no significant change was observed in the cortical bone. FPM treatment resulted in a tendency towards a slight decrease in BMD (Fig. 3B), Cs.Th (Fig. 3C), Ct.BV (Fig. 3D), and MMI (Fig. 3E) from Day 19, although these changes were not statistically significant. The corresponding absolute values of the experimental results are presented in Table 1.

FPM decreases the number of osteoclasts in mouse trabecular bone

Histological analysis of the distal femur confirmed our micro-CT findings of decreased BV/TV (Fig. 2C) and Tb.N (Fig. 2G) values in the FPM-treated group. To investigate the effect of FPM on the bone and number of osteoclasts, we performed histological staining of the femurs using H&E and TRAP stains. As shown in Fig. 4A, compared with the control group, the FPM-treated group showed a significant reduction in the femoral trabecular bone area (Fig. 4B). Additionally, the FPM-treated group had a significantly higher number of osteoclasts than that in the control group (Fig. 4C). These data consistently demonstrate the FPM-induced promotion of osteoclast differentiation, observed *in vitro,* and the bone loss in mice, observed in *in vivo* micro-CT analyses.

Low FPM concentrations promote osteoclast differentiation in BMMs

We hypothesised that FPM would enhance osteoclast differen-

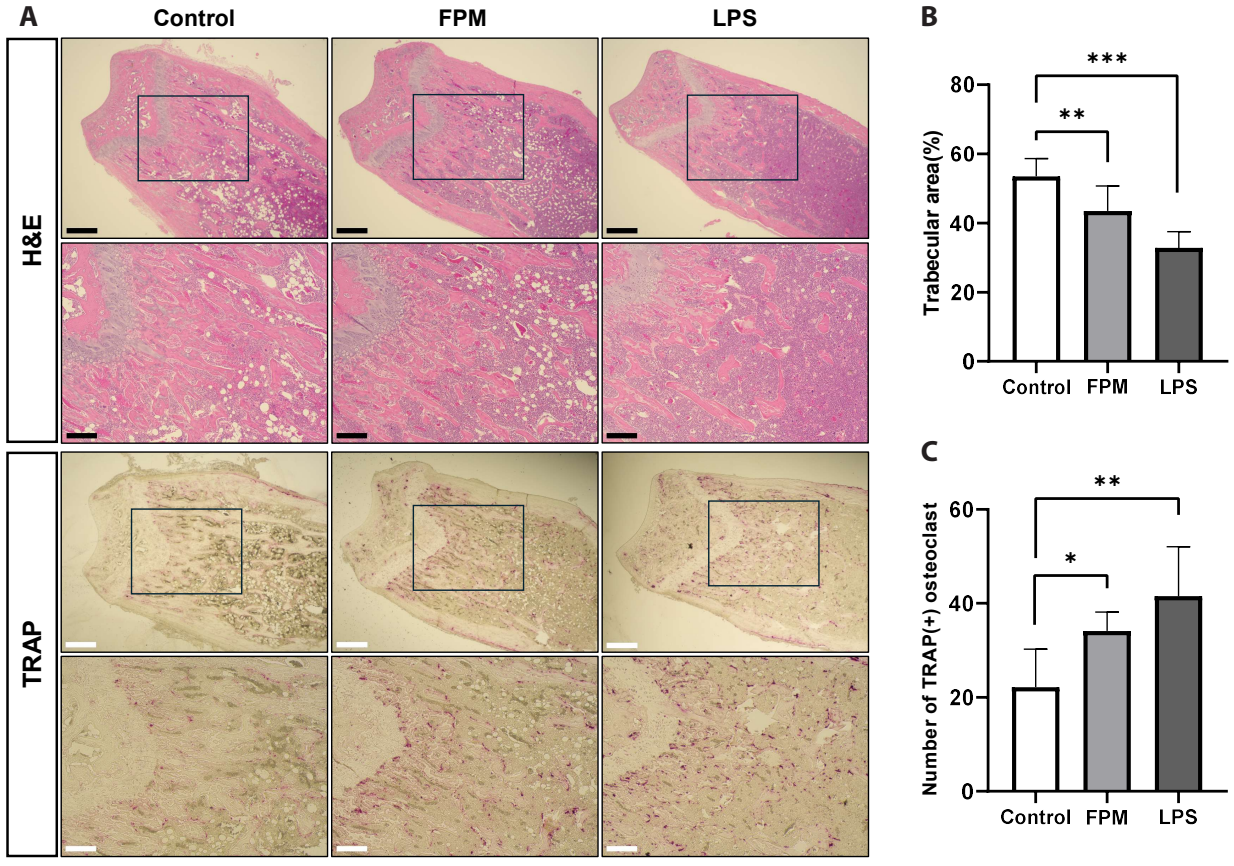

Fig. 4. Histological analysis of tissue sections from mouse femurs after fine particulate matter (FPM) exposure using haematoxylin and eosin (H&E) and tartrate-resistant acid phosphatase (TRAP) staining. Histological analysis was performed on femoral sections of mice on Day 19 after treatment (control group, n = 5, FPM-treated group, n = 7, and LPS-treated group, n = 3). (A) Representative images of H&E and TRAP staining from each group (40× and 100× magnification, Scale bars: 500 and 200 μm, respectively). (B) The trabecular area was measured using the ImageJ software. (C) The number of osteoclasts was counted using the ImageJ software. Bars represent mean ± standard deviation. LPS, lipopolysaccharide. *p < 0.05, **p < 0.01, ***p < 0.001 *vs*. control.

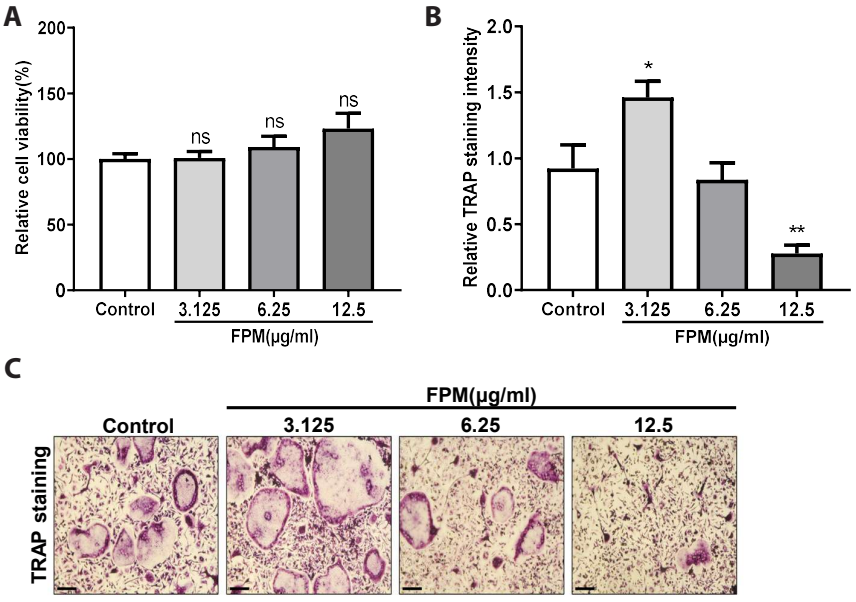

Fig. 5. Effect of fine particulate matter (FPM) on osteoclast differentiation in bone marrow-derived macrophages (BMMs). (A) Cell viability was determined using the MTS assay at various concentrations of FPM (0, 3.125, 6.25, and 12.5 μg/ml). (B) Analysis of the relative TRAP intensity in osteoclasts. BMMs were treated with various concentrations of FPM (0, 3.125, 6.25, and 12.5 μg/ml) or vehicle (PBS) in the presence of M-CSF (30 ng/ml) and RANKL (50 ng/ml) stimulation. TRAP intensity was measured using Image J software. (C) Osteoclasts were observed *via* TRAP staining. TRAP-positive cells were photographed under a light microscope. Scale bar, 100 μm. Bars represent mean ± standard deviation. All data were confirmed in three independent experiments. PBS, phosphate-buffered saline; M-CSF, macrophage-colony stimulating factor; RANKL, receptor activator of nuclear factor κB ligand; TRAP, tartrate-resistant acid phosphatase. *p < 0.05, **p < 0.01, ***p < 0.001 *vs*. control.

tiation in BMMs. Cells were cultured with various concentrations of FPM, M-CSF, and RANKL for 5 days. We confirmed that dose-dependent FPM treatment (3.125–12.5 μg/ml) did not induce cytotoxicity (Fig. 5A). To examine the effect of FPM on osteoclast differentiation, we performed a TRAP assay, wherein the highest TRAP intensity was observed at 3.125 μg/ml (Fig. 5B; representative image of TRAP staining in Fig. 5C). FPM showed a complete stimulatory effect at 3.125 μg/ml. Conversely, compared to that in the control, the TRAP intensity declined at 6.25 and 12.5 μg/ml. These results suggested that low concentrations of FPM promoted osteoclast differentiation in BMMs without cytotoxic effects.

DISCUSSION

FPM, which has been prevalent for quite some time, exerts deleterious effects on multiple organ systems, and ongoing research aims to investigate its effects. However, experimental studies have mostly focused on the respiratory system; few studies have explored the effects of FPM on other body systems. The previous studies on the relationship between FPM and bone health were mostly reviews or cohort studies [11,12]; thus, there is a lack of experimental or *in vivo* investigations. Therefore, this study aimed to address this gap by assessing the influence of FPM on bone remodelling, both *in vitro* and *in vivo*.

In the present study, micro-CT and histological analyses were conducted to assess the effects of FPM on bone structure. These results showed a significant reduction in trabecular BMD in the femur on Day 19, along with similar reductions in BV/TV and Tb.N in the FPM-treated group. BV/TV reflects changes in total bone volume, while Tb.N indicates the amount of trabecular bone per unit length. Tb.Th, a measure of trabecular bone thickness, showed a decreasing trend, suggesting diminished osteogenic activity although not statistically significant. Conversely, BS/BV and Tb.Sp increased with decreasing trabecular bone thickness. These findings, along with the reduction in Tb.N, suggest that FPM reduces osteogenic activity [25,26]. Moreover, histological analysis of the femoral bone revealed a reduction in the trabecular area and an increased number of osteoclasts in the FPM-treated group compared to the control group. Collectively, this study demonstrates that FPM exposure over time leads to lower BMD and osteogenicity in the mouse femur. This finding provides evidence supporting previous cohort and review studies that reported FPM-induced osteoporosis.

These findings are also consistent with the result on osteoclast cells *in vitro*, FPM influenced the differentiation of osteoclasts. While FPM addition had no negative impact on cell viability *in vitro* experiments, it significantly promoted osteoclast differentiation at low concentrations. Furthermore, since *in vivo* experiments using histological staining demonstrated that IP injection of FPM induces bone loss in the femoral trabecular bone of mice and increases the number of osteoclasts in the tissue, comprehensive analysis of these results can elucidate the potential pathways for FPM-induced osteoclast-mediated bone loss (Fig. 6). Follow-

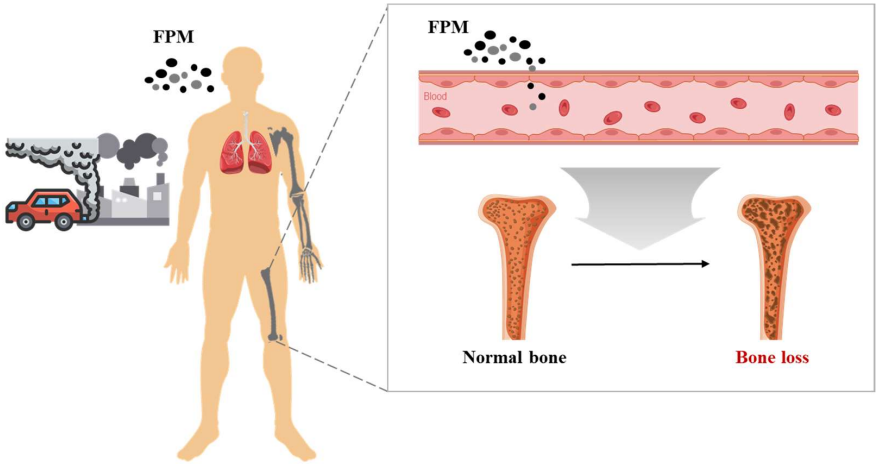

Fig. 6. Schematic diagram illustrating the potential pathway of fine particulate matter (FPM) induced osteoclast-mediated bone loss. People are frequently exposed to FPM in everyday life. FPM have the potential to induce bone loss by traversing the bloodstream to bones, where they can stimulate osteoclast differentiation and bone tissue resorption.

ing inhalation, FPM enters the bloodstream, facilitating the differentiation of precursor cells into osteoclasts and regulating their differentiation, activity, and survival to ultimately induce bone loss.

However, the *in vitro* results indicated that high concentrations of FPM decreased osteoclast differentiation. This indicates the possibility that high FPM concentrations reduce bone resorption, warranting further investigation. Several possibilities could be considered in this regard.

First, concentration-dependent effects should be considered. Although low concentrations of FPM lead to increased osteoclast differentiation, high FPM concentrations can cause excessive oxidative stress, which leads to cell damage and the inhibition of osteoclast survival and differentiation. Although the study demonstrated the absence of cytotoxicity from FPM exposure, the study did not explore the mechanisms underlying bone loss at different FPM concentrations. Therefore, other possibilities beyond concentration-dependent effects should be considered. Second, compared to cell experiments, the bone loss observed in animal experiments could be due to a prolonged exposure to FPM, which adversely affects the overall bone health more significantly. Chronic exposure to FPM continuously induces inflammatory responses, which, in the long term, leads to the predominance of bone resorption over bone formation. FPM-induced systemic inflammatory responses can impair the function of osteoblasts, which mediate bone formation, and this results in decreased bone formation and increased bone resorption that eventually causes bone loss. In future research, it will be necessary to examine the FPM-induced changes in osteoblasts in mouse bone tissue and investigate the experimental models and mechanisms of FPM-induced suppression of bone morphogenetic protein signalling and decreased osteoblast differentiation.

Several limitations in this study should be acknowledged. First, the use of IP injection to assess short-term FPM effects may not reflect chronic FPM exposure. Additionally, as only the IP route of administration was explored, other potential routes such as oropharyngeal aspiration, intranasal instillation, and intratracheal instillation may be neglected. Second, this investigation focused solely on osteoclasts with a small sample size. It may neglect the potential impact of FPM on osteoblast differentiation and the interplay between these cell types in bone homeostasis. In addition, *in vitro* findings may not fully translate to the *in vivo* environment. Future research should investigate the influence of FPM on osteoblast activity and osteoclast-osteoblast interactions in adequate sample size to gain a more comprehensive understanding of FPM's role in bone loss. Although this study was conducted with a small sample size, the results were reproducible and showed consistent statistically significant patterns within each group. This indicates that the findings of this study are reliable, especially given the consistent patterns observed in the LPS group, which was used as the positive control. The positive control played a crucial role in verifying the experimental system, providing a basis for comparison, and deriving the interpretation of results. We employed rigorous statistical analysis methods to minimize errors that could arise from a small sample size, thereby ensuring the reliability of the data despite the limited sample size. Future research will include a larger sample size to validate and expand upon the results presented in this study. Finally, extrapolation of these findings to humans necessitates caution due to the use of a mouse model. Future studies in humans, if feasible, would be of significant value. This comprehensive understanding of FPM's impact on bone health can be achieved by incorporating longer exposure durations, exploring diverse administration routes, investigating osteoblast-osteoclast interactions, and employing more precise methods to elucidate the underlying mechanisms.

In conclusion, this study investigated the impact of FPM on bone health in mice over a short period of time. The results

demonstrated that exposure to FPM had negative effects on bone health, inducing osteoclast-mediated bone loss *in vivo*. These findings provide a basis for future studies on the effects of FPM on bone health and highlight the importance of understanding the mechanisms of FPM exposure.

FUNDING

This research was funded by the National Research Foundation of Korea (NRF) grant funded by the Korean government (2022R1G1A1004843).

ACKNOWLEDGEMENTS

All figures are developed by the authors.

CONFLICTS OF INTEREST

The authors declare no conflicts of interest.

REFERENCES

1. World Health Organization. Ambient (outdoor) air pollution [Internet]. World Health Organization, 2022 [cited 2024 Feb 02]. Available from: https://www.who.int/news-room/fact-sheets/detail/ambient-(outdoor)-air-quality-and-health
2. Pope CA 3rd, Burnett RT, Thun MJ, Calle EE, Krewski D, Ito K, Thurston GD. Lung cancer, cardiopulmonary mortality, and long-term exposure to fine particulate air pollution. *JAMA*. 2002;287:1132-1141.
3. Bai Y, Sun Q. Fine particulate matter air pollution and atherosclerosis: mechanistic insights. *Biochim Biophys Acta*. 2016;1860:2863-2868.
4. Park EJ, Kim DS, Park K. Monitoring of ambient particles and heavy metals in a residential area of Seoul, Korea. *Environ Monit Assess*. 2008;137:441-449.
5. Kim KH, Kabir E, Kabir S. A review on the human health impact of airborne particulate matter. *Environ Int*. 2015;74:136-143.
6. Cho CC, Hsieh WY, Tsai CH, Chen CY, Chang HF, Lin CS. In vitro and in vivo experimental studies of $PM_{2.5}$ on disease progression. *Int J Environ Res Public Health*. 2018;15:1380.
7. Alfaro-Moreno E, Torres V, Miranda J, Martínez L, García-Cuellar C, Nawrot TS, Vanaudenaerde B, Hoet P, Ramírez-López P, Rosas I, Nemery B, Osornio-Vargas AR. Induction of IL-6 and inhibition of IL-8 secretion in the human airway cell line Calu-3 by urban particulate matter collected with a modified method of PM sampling. *Environ Res*. 2009;109:528-535.
8. Yang W, Omaye ST. Air pollutants, oxidative stress and human health. *Mutat Res*. 2009;674:45-54.
9. Salari N, Ghasemi H, Mohammadi L, Behzadi MH, Rabieenia E, Shohaimi S, Mohammadi M. The global prevalence of osteoporosis in the world: a comprehensive systematic review and meta-analysis. *J Orthop Surg Res*. 2021;16:609.
10. Li H, Xiao Z, Quarles LD, Li W. Osteoporosis: mechanism, molecular target and current status on drug development. *Curr Med Chem*. 2021;28:1489-1507.
11. Yang Y, Li R, Cai M, Wang X, Li H, Wu Y, Chen L, Zou H, Zhang Z, Li H, Lin H. Ambient air pollution, bone mineral density and osteoporosis: Results from a national population-based cohort study. *Chemosphere*. 2023;310:136871.
12. Ranzani OT, Milà C, Kulkarni B, Kinra S, Tonne C. Association of ambient and household air pollution with bone mineral content among adults in peri-urban South India. *JAMA Netw Open*. 2020;3:e1918504.
13. Tian Y, Hu Y, Hou X, Tian F. Impacts and mechanisms of $PM_{2.5}$ on bone. *Rev Environ Health*. 2023. doi: 10.1515/reveh-2023-0024. [Epub ahead of print]
14. von Scheidt M, Zhao Y, Kurt Z, Pan C, Zeng L, Yang X, Schunkert H, Lusis AJ. Applications and limitations of mouse models for understanding human atherosclerosis. *Cell Metab*. 2017;25:248-261.
15. He M, Ichinose T, Yoshida S, Ito T, He C, Yoshida Y, Arashidani K, Takano H, Sun G, Shibamoto T. PM2.5-induced lung inflammation in mice: differences of inflammatory response in macrophages and type II alveolar cells. *J Appl Toxicol*. 2017;37:1203-1218.
16. Montenegro M. 2023 world air quality report [Internet]. IQAir, 2024 [cited 2024 Feb 10]. Available from: https://www.iqair.com/newsroom/waqr-2023-pr
17. Tang W, Huang S, Du L, Sun W, Yu Z, Zhou Y, Chen J, Li X, Li X, Yu B, Chen D. Expression of HMGB1 in maternal exposure to fine particulate air pollution induces lung injury in rat offspring assessed with micro-CT. *Chem Biol Interact*. 2018;280:64-69.
18. Tang W, Du L, Sun W, Yu Z, He F, Chen J, Li X, Li X, Yu L, Chen D. Maternal exposure to fine particulate air pollution induces epithelial-to-mesenchymal transition resulting in postnatal pulmonary dysfunction mediated by transforming growth factor-β/Smad3 signaling. *Toxicol Lett*. 2017;267:11-20.
19. Park SR, Lee JW, Kim SK, Yu WJ, Lee SJ, Kim D, Kim KW, Jung JW, Hong IS. The impact of fine particulate matter (PM) on various beneficial functions of human endometrial stem cells through its key regulator SERPINB2. *Exp Mol Med*. 2021;53:1850-1865.
20. Jo YJ, Lee HI, Kim N, Hwang D, Lee J, Lee GR, Hong SE, Lee H, Kwon M, Kim NY, Kim HJ, Park JH, Kang YH, Kim HS, Lee SY, Jeong W. Cinchonine inhibits osteoclast differentiation by regulating TAK1 and AKT, and promotes osteogenesis. *J Cell Physiol*. 2021;236:1854-1865.
21. Kim M, Park JH, Go M, Lee N, Seo J, Lee H, Kim D, Ha H, Kim T, Jeong MS, Kim S, Kim T, Kim HS, Kang D, Shim H, Lee SY. RUFY4 deletion prevents pathological bone loss by blocking endo-lysosomal trafficking of osteoclasts. *Bone Res*. 2024;12:29.
22. Lee SK, Park KK, Park JH, Lim SS, Chung WY. The inhibitory effect of roasted licorice extract on human metastatic breast cancer cell-induced bone destruction. *Phytother Res*. 2013;27:1776-1783.
23. Lee DC, Oh JM, Choi H, Kim SW, Kim SW, Kim BG, Cho JH, Lee J, Kim JS. Eupatilin inhibits reactive oxygen species generation via Akt/NF-κB/MAPK signaling pathways in particulate matter-exposed human bronchial epithelial cells. *Toxics*. 2021;9:38.
24. Roberts BC, Arredondo Carrera HM, Zanjani-Pour S, Boudiffa M,

Wang N, Gartland A, Dall'Ara E. PTH(1-34) treatment and/or mechanical loading have different osteogenic effects on the trabecular and cortical bone in the ovariectomized C57BL/6 mouse. *Sci Rep*. 2020;10:8889.

25. Lee JH, Chun KJ, Kim HS, Kim SH, Han P, Jun Y, Lim D. Alteration patterns of trabecular bone microarchitectural characteristics induced by osteoarthritis over time. *Clin Interv Aging*. 2012;7:303-312.
26. Sulaiman SZS, Tan WM, Radzi R, Shafie INF, Ajat M, Mansor R, Mohamed S, Ng AMH, Lau SF. Comparison of bone and articular cartilage changes in osteoarthritis: a micro-computed tomography and histological study of surgically and chemically induced osteoarthritic rabbit models. *J Orthop Surg Res.* 2021;16:663.